Special Collection

Enhancement of Functional Properties of Liquid Electrolytes for Lithium-Ion Batteries by Addition of Pyrrolidinium-Based Ionic Liquids with Long Alkyl-Chains

Arcangelo Celeste,[a, b] Laura Silvestri,*[c] Marco Agostini,[d] Matthew Sadd,[d] Stefano Palumbo,[a] Jaya Kumar Panda,[a] Aleksandar Matic,[d] Vittorio Pellegrini,[a] and Sergio Brutti*[e]

Three ionic liquid belonging to the *N*-alkyl-*N*-methylpyrrolidinium bis(trifluoromethanesulfonyl) imides ($Pyr_{1,n}TFSI$ with $n=4,5,8$) have been added as co-solvent to two commonly used electrolytes for Li-ion cells: (a) 1 M lithium hexafluorophosphate ($LiPF_6$) in a mixture of ethylene carbonate (EC) and linear like dimethyl carbonate (DMC) in 1:1 v/v and (b) 1 M lithium bis-(trifluoromethanesulfonyl)imide (LiTFSI) in EC:DMC 1:1 v/v. These electrolyte formulations (classified as P and T series containing $LiPF_6$ or LiTFSI salts, respectively) have been analyzed by comparing ionic conductivities, transport numbers, viscosities, electrochemical stability as well as vibrational properties. In the case of the $Pyr_{1,5}TFSI$ and $Pyr_{1,8}TFSI$ blended formulations, this is the first ever reported detailed study of their functional properties in Li-ion cells electrolytes. Overall, P-electrolytes demonstrate enhanced properties compared to the T-ones. Among the various P electrolytes those containing $Pyr_{1,4}TFSI$ and $Pyr_{1,5}TFSI$ limit the accumulation of irreversible capacity upon cycling with satisfactory performance in lithium cells.

1. Introduction

Nowadays, lithium-ion batteries (LIBs) represent the technology of choice to power small portable devices such as laptop and cell phones, electric vehicles and large stationary application systems.[1] Researchers are continuously focused on the investigation of new chemistries for electrodes to further improve power and energy density beyond current commercial formulations, as well as enhancing the overall safety of those storage devices.[2] Among the different components of LIBs, the electrolyte represents a critical one that affect both safety and cell performance.[3] Commercially available electrolyte consists of a mixture of carbonate-based dipolar aprotic solvents dissolving a lithium salt. Concentrated solutions of lithium hexafluorophosphate ($LiPF_6$) dissolved in a mixture of cyclic carbonates like ethylene carbonate (EC) and linear like dimethyl carbonate (DMC) in 1:1 v/v (LP30, Merck), are the most commonly used one for commercial LIBs, thanks to the good ionic conductivity, chemical inertness, wide electrochemical stability window and the ability to passivate aluminum current collectors.[4,5] However, the $LiPF_6$ salt is thermally unstable, spontaneously decomposes to form LiF and PF_5 species and easily hydrolyze with water traces forming HF.[6,7] Feasible alternatives to replace $LiPF_6$ are lithium imide salts, like LiTFSI (lithium bis-(trifluoromethanesulfonyl)imide).[8,9] Nevertheless, despite LiTFSI is less prone to hydrolysis and possess higher thermal and electrochemical stabilities compared to $LiPF_6$,[10,11] it is corrosive toward the aluminum current collector,[12] thus hindering its use in a commercial device.

Turning to solvents, alkyl carbonates used as solvents are highly flammable, volatile and toxic.[13,14] Their substitution with low flammable ionic liquids (ILs) have been proved to reduce the risk of thermal runaway and overall hazard of LIBs.[15–18] ILs are low-temperature molten salts, usually formed by a large ammonium quaternary cation and a charge delocalized anion. They have been intensively studied as potential electrolyte solvents in batteries, thanks to their advantageous properties such as the low vapor pressure, thermal stability in a wide temperature range and high ionic conductivity.[19–21] However, after the addition of lithium salt, IL-based electrolytes show

[a] A. Celeste, S. Palumbo, Dr. J. K. Panda, Dr. V. Pellegrini
Graphene labs
Istituto Italiano di Tecnologia
Via Morego 30, 16163,Genova, Italy
[b] A. Celeste
Dipartimento di Chimica e Chimica Industriale
Università degli Studi di Genova
Via Dodecaneso 31, 16146 Genova, Italy
[c] Dr. L. Silvestri
Dipartimento di Tecnologie Energetiche
ENEA, C.R. Casaccia
Via Anguillarese 301, 00123 Roma, Italy
E-mail: laura.silvestri@enea.it
[d] Dr. M. Agostini, M. Sadd, Dr. A. Matic
Department of Physics
Chalmers University of Technology
SE41296 Göteborg, Sweden
[e] Dr. S. Brutti
Dipartimento di chimica
Sapienza Università di Roma
Piazzale Aldo Moro 5, 00185Roma, Italy
E-mail: sergio.brutti@uniroma1.it

Supporting information for this article is available on the WWW under https://doi.org/10.1002/batt.202000070

Special Collection *An invited contribution to a Special Collection on Electrolytes for Electrochemical Energy Storage*

high viscosity resulting in unsatisfactory ionic conductivity and Li^+ transport number.[22–26] To overcome these issues, a common strategy is the addition of an IL to an organic solvents-based electrolytes.[27–31] Several works demonstrated the synergistic effect of the two components leading to lower viscosity, higher conductivity at room temperature as well as improved safety in terms of thermal stability and flammability.[17,18,29,30,32–38] The IL organic solvent based electrolytes results in a good compromise between safety and conductivity and it represent an advantage in terms of costs, compared to the use of pure ILs.

Here, we investigate the physico-chemical properties of six (6) IL-added electrolytes, obtained adding to the 1 M $LiPF_6$ in EC:DMC = 1:1 v/v and to the 1 M LiTFSI in EC:DMC = 1:1 v/v, *N*- alkyl-*N*-methyl pyrrolidinium based-IL with different length of alkyl chain. Our goal is to study the influence of the cation size on their physical-chemical and electrochemical properties. The chemical formula and structural representations of solvent molecules as well as ILs constituents' anions and cations are shown in the Figure 1 for clarity. Besides the $Pyr_{1,4}$TFSI ionic liquid, that has been studied previously also by us as co-solvent in electrolytes for Li-ion batteries (see ref.), this is the first ever reported detailed study of the functional properties of 4 new electrolyte formulations, i.e. $Pyr_{1,5}$TFSI and $Pyr_{1,8}$TFSI ILs added to the 1 M $LiPF_6$ in EC:DMC = 1:1 v/v and to the 1 M LiTFSI in EC:DMC = 1:1 v/v starting solutions.

The manuscript is organized in four main sections where (a) flammability and electrochemical stability, (b) transport properties, (c) electrolyte molecular structure by Raman spectroscopy and (d) full Li-ion proof-of-concept are presented and discussed.

2. Results and Discussion

Six (6) electrolyte solutions have been prepared by the addition of 3 different ILs in a 1:1 weight ratio to two carbonates-based electrolytes, i.e. 1 M LiTFSI in EC:DMC = 1:1 v/v and 1 M $LiPF_6$ in EC:DMC = 1:1 v/v. The ILs are formed by the bis(tri-fluoro methane sulfonyl)imide (TFSI) anion and *N*-alkyl-*N*-methyl-pyrrolidinium ($Pyr_{1,x}$) cations where the alkyl chain is buthyl-, penthyl- and octyl- ($Pyr_{1,4}$, $Pyr_{1,5}$ and $Pyr_{1,8}$, respectively), as reported in Figure 1. All the electrolyte solutions are summarized in the Table 1 with the corresponding coding adopted thereafter.

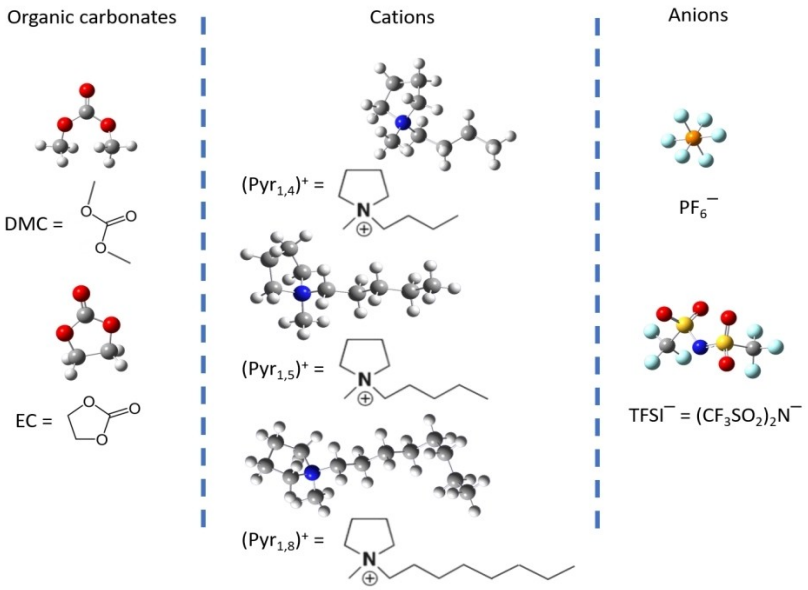

Figure 1. Chemical formula and structural representations of solvent molecules and ILs constituents anions and cations.

Table 1. Compositions of the electrolyte solutions under investigation.

Label	Lithium salt	Solvent	Salt molality	Ionic liquid	IL [wt.%]
T	LiTFSI	EC:DMC = 1:1 v/v	0.98	–	–
TA	LiTFSI	EC:DMC = 1:1 v/v	0.43	$[Pyr_{1,4}]$TFSI	50
TB	LiTFSI	EC:DMC = 1:1 v/v	0.43	$[Pyr_{1,5}]$TFSI	50
TC	LiTFSI	EC:DMC = 1:1 v/v	0.43	$[Pyr_{1,8}]$TFSI	50
P	$LiPF_6$	EC:DMC = 1:1 v/v	0.87	/	/
PA	$LiPF_6$	EC:DMC = 1:1 v/v	0.41	$[Pyr_{1,4}]$TFSI	50
PB	$LiPF_6$	EC:DMC = 1:1 v/v	0.41	$[Pyr_{1,5}]$TFSI	50
PC	$LiPF_6$	EC:DMC = 1:1 v/v	0.41	$[Pyr_{1,8}]$TFSI	50

2.1. Flammability and Electrochemical Stability

Flammability properties of the 6 electrolytes solutions have been obtained through the evaluation of flash point. According to "European CLP regulation"[39] the flash point is considered as a determinant parameter to classify the flammable liquids. Figure 2 reports the values for the P and T electrolytes solutions. The values of electrolytes before the addition of ILs (P and T) have been added for comparison.

The pristine P and T electrolytes show very similar flash points close to room temperature (≈28 °C). On the other hand, after the addition of IL all the blended electrolytes show T_{flash} above 40 °C, in some cases approaching 50 °C.

Overall all IL-added electrolytes show mitigated flammability compared to benchmarks with pure alkyl carbonate solvents, demonstrating that the flammability of carbonates-based electrolytes can be successfully reduced with the addition of pyrrolidinium-based ionic liquids with a beneficial trend with the elongation of alkyl chains. It is remarkable to underline that the "Recommendations on the Transport of Dangerous Goods, Manual of Tests and Criteria of United Nations Organization (UNO)"[40] indicates that liquids with flash points higher than 35 °C are not classified in Category 3 (flammable liquids). All the here proposed new electrolyte formulations are above this threshold whereas both commercial pristine carbonate-electrolytes are below.

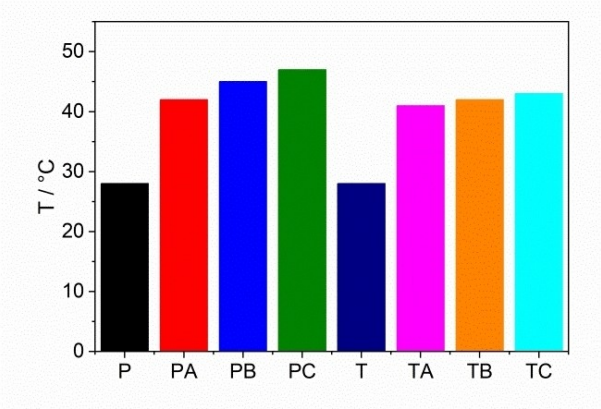

Figure 2. Flash points tests for the P- and T-based electrolytes solutions.

Table 2. Irreversible reaction potentials measured for anodic and cathodic scan.

Label	Anodic scan onset potential [V]	Cathodic irreversible decomposition potentials [V]	
		Onset	Peak edge
P	5.1	0.77	0.37
PA	5.45	0.7	0.35
PB	5.4	0.73	0.49
PC	5.3	0.7	0.45
T	4.9	0.82	0.37
TA	5.4	0.82	0.42
TB	5.2	0.75	0.4
TC	4.6	0.74	0.44

Electrochemical stability windows of the benchmark and IL-added electrolyte have been evaluated by Linear Sweep Voltammetry (LSV) and Cyclic Voltammetry (CV). The anodic/cathodic potentials for the irreversible reactions are summarized in Table 2. The anodic LSVs and the cathodic CV are shown in the supplementary material (Figure S1 and S2, respectively).[15,30,31,35,41]

In all the electrolytes, we can observe a small pre decomposition peak above 4.5 V, followed by a current drift above 5 V (Figure S1a–b). This peak is particularly evident in the case of the [$Pyr_{1,8}$]TFSI added electrolytes. In particular, all the P-electrolytes exhibit a current drift above 5.2 V due to the irreversible degradation of the solvent molecules: however, the addition of IL in the alkyl-carbonates solvent slightly alters anodic stability. In particular, a shift to higher voltages in the onset potential is observed for PA and PB electrolytes, while in the case of PC the onset potential is slightly decrease compared to the P one. As expected, the T electrolyte exhibits a lower anodic stability compared to P electrolyte[11] being the onset potential shifted to lower voltages. On the other hand, in the case of the TC electrolyte the anodic stability slightly decreases, being the onset potential shifted to smaller voltages compared to the T benchmark.

Turning to the cathodic branch, as expected the P electrolyte shows multiple electro-active processes:[14] (a) a small current drift starting at around 1.3 V, followed by other signals with onset potentials at (b) 0.77, (c) 0.54 and (d) ~0.2 V in the first voltammetric cycle. Generally speaking, the addition of all ILs shifts the reduction onset potentials downward to lower voltages, thus enlarging the cathodic stability windows. In all T and P-electrolytes, as expected, in the following voltammetry cycles, the peak centered at ~0.5 V disappears (Figure S2b and S2c), being originated by the decomposition of the electrolyte components on electrode surface. This is a clear evidence of the formation of an electrochemically stable solid-electrolyte interface (SEI). In summary the addition of ILs to both P and T electrolytes extends the electrochemical stability window achieving a remarkable 0.75–5.2 V vs. Li and 0.75–5.4 V vs. Li stability ranges for TB and PB, respectively.

2.2. Transport Properties

The ionic conductivity of the IL-based electrolytes and the T and P benchmarks have been measured in the temperature range between 60 to −20 °C as shows in the Figure 3a–b. The drops conductivity values have a similar trend for both the T and P benchmark solutions above 0 °C, while the ionic conductivity more for the $LiPF_6$ based solution below 0 °C. As already reported in the literature,[17,18,29,30,32–38] the addition of ILs slightly decrease the conductivity. In fact, both the IL-added T- and P-electrolytes show smaller values compared to the T and P benchmarks with a decreasing trend that follows the size of the alkyl chain being TC < TB < TA < T and PC < PB < PA < P. Contrary to the data reported by Guerfi et al.[29] the addition of 50% of IL in the electrolytes leads to a decrease of ionic conductivity, despite a similar trend is observed for viscosity, as

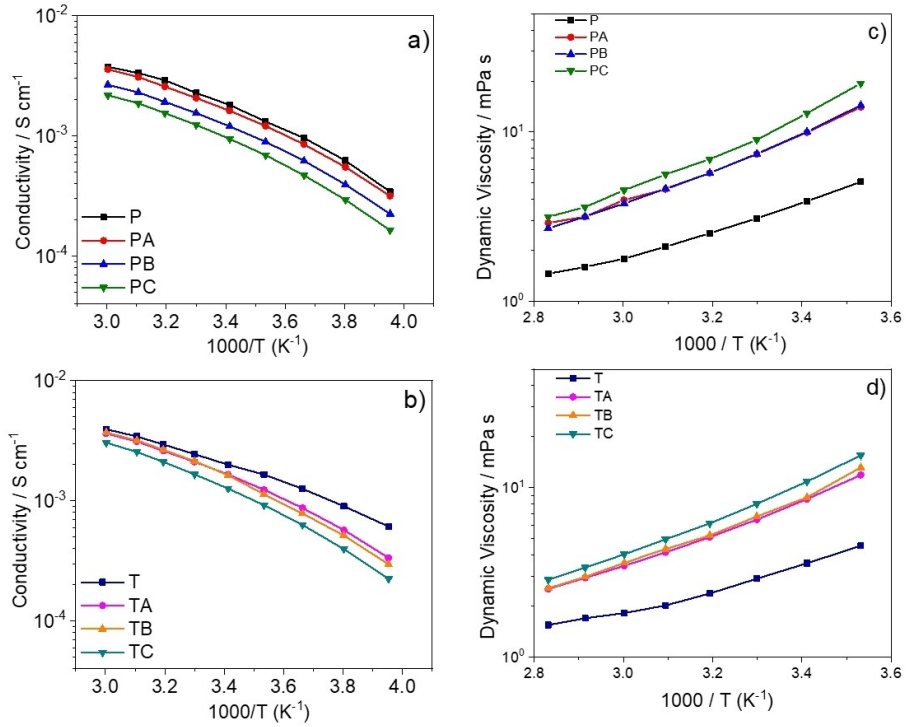

Figure 3. Arrhenius plots of the P-series electrolytes (a) and T-series electrolytes (b) in the temperature range from 60 °C to −20 °C and Dynamic viscosity as function of the temperature for the P-series electrolytes (c) and T-series electrolytes (d) in the temperature range from 10 °C to 80 °C.

reported in Figure 3c–d. In fact, the dynamic viscosities show a reverse trend in respect to conductivity (see Figure 3c–d).[29] In all cases the addition of an ILs increase the viscosity of the solution. Moreover, in line with the conductivities also viscosities of IL-added electrolytes show a trend with the size of the alkyl chain in the pyrrolidinium cation being TC > TB > TA > T and PC > PB > PA > P. These data are partially in line with the observation of Oldiges et al.:[42] the ionic conductivity in the mixture of ionic liquids/organic solvent is affected mostly by the increasing of viscosity. This description nicely matches with the here reported reversed trend of various electrolytes viscosities and conductivities. Going further, alterations in viscosities and conductivities likely roots in the modification of the lithium coordination in the solution induced by ILs.

The evolution in temperature of the ionic conductivity (σ) of the two series of novel electrolytes is well fitted with the Vogel-Tammann-Fulcher (VTF) equation [Eq. (1)], commonly used for IL-based liquids:[43,44]

$$\sigma = \sigma_0 \cdot exp\{-E_a/[R \cdot (T - T_0)]\}$$

Where the pre-exponential term σ_0 corresponds to the ionic conductivity at infinite temperature, E_a is a pseudo-activation energy for the ion hopping and T_0 is defined as the ideal glass transition temperature below which the ion mobility is zero. Besides the VTF model, also the Arrhenius equation can be used to fit the temperature dependence of the ionic conductivity in liquids.[45] The comparison among the fitting convergence parameters (R2 and chi-square sums) obtained for the two models for all the eight electrolytes are summarized in the supplementary material (table S1). Overall, the VTF model outperform the fitting by the Arrhenius equation of more than one order of magnitude in convergences for all cases. Therefore, we discarded the fittings by the Arrhenius model and assumed the VTF one in line with the standard literature.[43,44]

The parameters obtained by the VTF linear fits for the conductivity trends with temperature are shown in Table 3.

The pseudo-activation energies increase while adding the ILs to both P and T electrolytes, apart for the TA case. On the other hand, the ideal glass transition temperatures decrease for the IL-added P-electrolytes while increase for the IL-added T-ones. One may speculate that the addition of ionic liquids may lead to a stronger binding energy between solvated ionic couples thus slightly hinders their individual mobility. Less clear is the missing matching between the evolution of the ideal

Table 3. Conductivity fitting coefficients calculated for the electrolyte solutions under investigation adopting a VTF model equation.

Label	Activation energy [kJ/mol]	Ideal glass transition temperature [Ke]
P	35	186
PA	44	176
PB	43	179
PC	47	177
T	47	157
TA	45	174
TB	54	168
TC	54	167

glass transition temperatures and the trend of standard entropies of mixing for the various electrolytes (T: 9.3 $J K^{-1} mol^{-1}$; T: 9.4 $J K^{-1} mol^{-1}$; PA, PB, PC: ~14 $J K^{-1} mol^{-1}$; TA, TB, TC: ~12 $J K^{-1} mol^{-1}$). The increase in the disorder of the liquid solution induced by the increase of the constituent species apparently extend the liquid range only in the case of the PA–PB and PC whereas the VTF fits suggest that TA, TB and TC electrolytes glassify at higher temperatures, from 10 to 15 degrees, compared to the benchmark T-one.

The ionicity of the IL-added electrolytes has been qualitatively checked by Walden rule in line with the majority of the literature approaches:[46–49]

$$\Lambda\eta = k$$

Where Λ is the molar conductivity, η the viscosity and k is a constant dependent from temperature. Figure 4 reports the Walden plot in which the log of viscosity is correlated to the log of conductivity. The straight line on the plot passing through the origin represents the "ideal Walden line" and it is referred to a 0.01 N KCl aqueous solution and can be used as calibration line.

All the IL added electrolytes are located well below the ideal Walden line, behaving as poor ionic liquids.[50] Furthermore, we can observe that all the IL-added electrolytes show similar ionicity slightly increased compared to the bare P and T electrolytes.

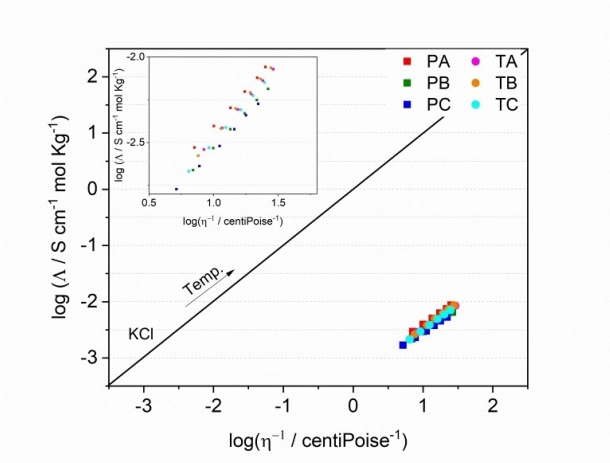

Figure 4. Walden plot for the IL-electrolyte mixtures.

2.3. Raman Spectroscopy Analysis

Raman spectroscopy has been used to investigate the interaction of lithium with TFSI anion of ionic liquid (see Figure 5 and Figures S3 in the supplementary material). Preliminary analysis has been made on pure ionic liquids, in order to identify any changes due to the different alkyl chains. Figure S3 (a–c) shows the Raman spectra acquired in 3 different spectral regions: 2700–3200 cm^{-1}, 725–755 cm^{-1} and 200–450 cm^{-1}. In the region between 2700–3200 cm^{-1} (Figure S3a) it is possible to detect the C–H vibrational modes derived from cation.

As consequence of the increasing of alkyl chain, the peak at and 2933 and at 2970 cm^{-1} exhibits modifications in the intensity of the vibrational modes, being this band associated to the modes of the alkyl chain.[51] Further differences can be

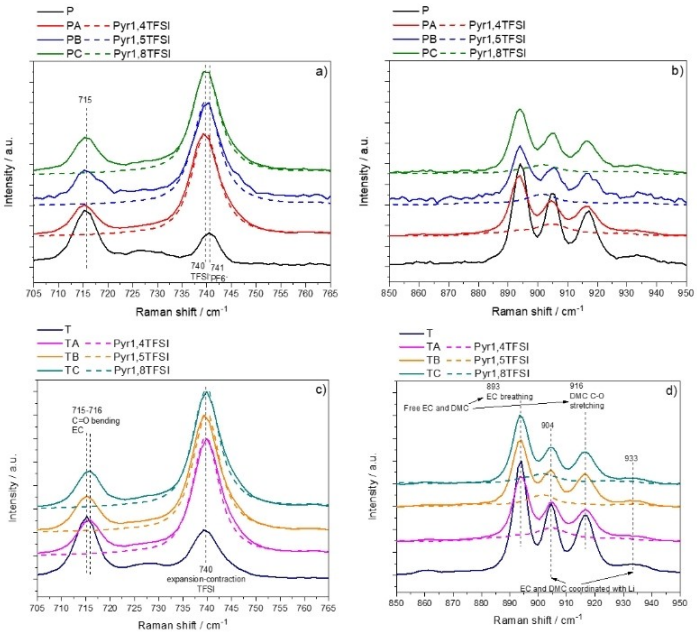

Figure 5. Raman spectra of the P-series electrolytes (a,b) and T-series electrolytes (c,d). Dotted lines correspond to the spectra acquired for the pure ionic liquids.

observed at 2852 cm^{-1} where $Pyr_{1,8}$TFSI exhibit a strong peak. The modes at 2876 and 2941 cm^{-1} in $Pyr_{1,4}$TFSI are shifted to lower wave numbers in $Pyr_{1,8}$TFSI, respectively to 2870 and 2933 cm^{-1}.[51] These bands are associated to the vibrational mode of CH_2 in ring. The shifts observed is indirectly correlated to the length of alkyl chain; but they depend more from the different position of $TFSI^-$ anion respect to the pyrrolidinic ring when the alkyl chain of cation increase. Furthermore, other bands with weak relative intensity can be detected at 3000 and 3031 cm^{-1} and related to the anti-symmetric stretching mode of C–H in $C–CH_3$ and $N^+–CH_3$, respectively.

The other two regions showed in figure S3b and c, are related to the vibrational mode of TFSI anion.[52,53] As evident in figure S3b, the 3 ionic liquids exhibit a strong peak at 740 cm^{-1} corresponding to the expansion-contraction modes of the whole anion. As expected,[52,53] negligible differences are detected in the three samples. Finally, the bands in the region 250–350 cm^{-1} showed in Figure S3c can be assigned to the twisting and rocking modes of SO_2 and CF_3 groups in the TFSI anion and are sensitive to the two stable conformers (cisoid and transoid).[52,53] In Figure 5 magnifications of the Raman spectra for all the electrolytes are shown in the ranges 850–950 cm^{-1} and 705–765 cm^{-1}. These spectral regions are typically used to investigate the coordination of Li^+ with TFSI anion and with the organic solvents, respectively.[53–57] The region between 850–950 cm^{-1}, showed in Figures 5b and 5d, exhibits a series of bands assigned to the vibrational modes of carbonate molecules.

According to literature,[53] the peaks at 893 and 916 cm^{-1} correspond to the EC breathing and C–O stretching of DMC for the free solvents, respectively. These bands are shifted respectively at 904 and 933 cm^{-1} when solvent molecules coordinate lithium ions.[42,58] In the case of electrolytes without ionic liquids, the three bands at 893, 904 and 916 cm^{-1} are sharp. On the contrary in all IL-added electrolytes the intensity of the bands in the 850–950 cm^{-1} region is reduced and all peaks are broader, especially in the band at 893 cm^{-1}. Furthermore, the peak broadening is more extended in all P-series electrolytes compared to the T-series, possibly suggesting a more disordered Li^+ coordination environment. In Figures 5a and 5c two major vibrational modes are found at 715 cm^{-1} and 740 cm^{-1}, corresponding to the C=O bending of EC and the expansion-contraction mode of the whole PF_6^- or TFSI anions, respectively. After the addition of ionic liquids for all the electrolyte solutions the band at 715 cm^{-1} decreases in relative intensity, broadens and slightly shifts to higher wave numbers. Regarding the vibrational mode at 740 cm^{-1}, in the P-electrolytes (Figure 5a) the small peak corresponding to PF_6^- anion in the EC/DMC $LiPF_6$ is completely overlapped with the strong band of the TFSI anion. On the contrary, in the T-electrolyte (Figure 5c) this peak increases in intensity and remains centered without relevant shifts. The strong band at 740 cm^{-1}, fingerprint of TFSI anion bending, is not affected by the presence of lithium salts, either LiTFSI or $LiPF_6$, nor by the length of the alkyl chain of the pyrrolydinium cation.

These vibrational features suggest, in line with previous experimental reports,[53,54,58] that Li^+ is preferentially coordinated by the C=O groups of the carbonate molecules, whereas TFSI is present as free anion. These spectral regions have been also used to perform a quantitative analysis about the coordination of Li^+ by a fitting procedure (see Supporting Information for the details). Specifically, the range 850–950 cm^{-1} was deconvoluted in 4 bands, accounting the free and coordinated EC and DMC.[42,58] Considering that in this region few vibrational features due to pyrrolidinium cation are also present and according to the previous works, these contributions have been subtracted.[42,58] In the range 705–765 cm^{-1} five bands have been included in the fitting, considering the free and coordinated EC and TFSI and the two conformers (cisoid and transoid) of TFSI (Figure S4).[42,58] In order to evaluate the population ratio of the two conformers of TFSI, i.e. cisoid and transoid, the spectral range 250–350 cm^{-1} was used (Figure S4).[56] Finally, in the case of P-series electrolytes, we also considered that PF_6^- band at 741 cm^{-1} that overlaps with the TFSI signal. In line with Oldiges et al.[42] we assumed constant the PF_6^- contribution in the composite electrolytes, including in the fitting the pristine peak from LP30 (Figure S5).

Figure 6 report the quantitative analysis as average coordination number of EC, DMC and TFSI with Li^+. In the IL free P electrolyte (Figure 6a), lithium ions are coordinated by 2.8 EC and 1.5 DMC molecules. Similar is the behavior for T (Figure 6b), where EC and DMC coordinates 2.4 and 1.7 Li-ions, respectively.

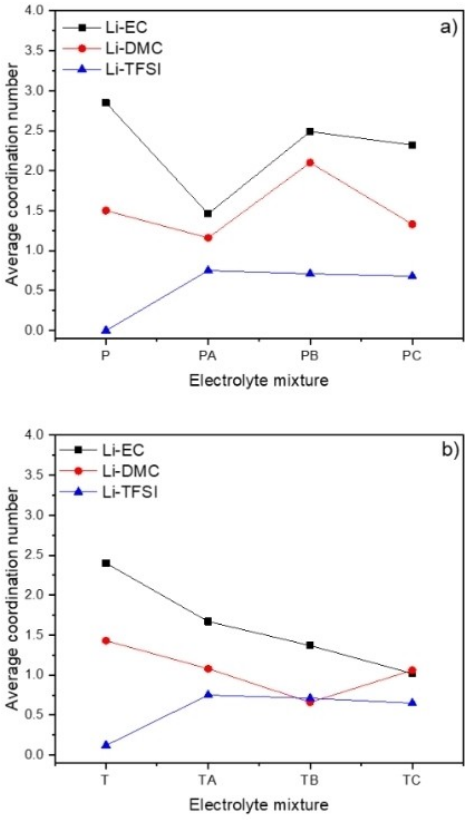

Figure 6. Lithium average coordination number for a) P– and b) T– electrolytes.

Furthermore, TFSI anion in T electrolyte is mostly found as free anion, demonstrating a weak interaction with lithium ions. When IL is added, the interaction between TFSI anion and Li^+ is around 0.75 either for PA and TA and it is only slightly modified changing the IL. Overall T-electrolytes show a weaker lithium coordination trend with the lengthening of alkyl chain, whereas in P-electrolytes the coordination numbers appear scattered.

2.4. Full Li–Ion Proof of Concept

As a final point of this study, the applicability in lithium cell of all these new electrolytes have been proved using a well-known cathode material such as $LiFePO_4$ (LFP) as shown in the supplementary information (Figure S7). When P is used as electrolyte, LFP shows a stable cycling along the first 60 cycles, developing a specific capacity of about 175 $mAhg^{-1}$ (Figure S7a–b). Nevertheless, prolonging cycling leads to failure of the cell with irreversible loss of capacity (Figure S7a). Despite capacity values are slightly decreased compared to the pure carbonate electrolytes, the IL solutions show good cycling stability in discharge-recharge tests and, more remarkably, the reversibility resulted improved, as demonstrated by cumulative irreversible capacity plots (Figure S8). In fact, while for P electrolyte after 40 cycles, a cumulative irreversible capacity of almost 120 $mAhg^{-1}$ is achieved, the latter doesn't exceed 75 $mAhg^{-1}$ when IL is added. This effect is particularly evident for PB electrolyte, in which the Coulombic Irreversible Capacity (CIC) is less than 45 $mAhg^{-1}$ after 40 cycles. Moving to the T-series electrolytes, Figures S7c–d showed the electrochemical performance obtained in Li/LFP cell. The performance of LFP with T electrolyte shows a stable capacity of $\approx$180 $mAhg^{-1}$. Similarly to P-series electrolytes, the addition of ionic liquids leads to decrease of capacity values. However, by the analysis of the plot in Figure S8, cumulative irreversible capacity present further decrease in comparison to P-based electrolytes and this is particularly evident in TA and TB electrolytes, with a CIC of only 15 $mAhg^{-1}$ after 40 cycles. From the analysis reported above, PB and TB resulted the best choice to verify the applicability of these kind of IL-added electrolytes in a Li-ion cell.

Before tests in full cell, also the electrochemical behavior of Si-graphene composite[59,60] electrodes with PB and TB electrolytes have been evaluated and the results reported in Figure S9. According to the reference[59] galvanostatic discharge-recharge tests were carried out using a current density of $\approx$C/10 (1 C = 350 mAg^{-1}) in a potential range of 0.1–1 V. A formation cycle between 0.01–2 V was added before any cycling to stabilize electrode-electrolyte interphase.[60] Potential profiles of the electrodes obtained during the formation cycle are reported in Figure S9b–d. The performance with P and T electrolytes has been added as reference. During formation (Figure S9b–d), the typical voltage profile of silicon-based anodes is visible with all the electrolytes: a long plateau below 0.1 V upon discharge followed by a slope around 0.2 V and a small plateau at 0.4 V. With both PB and TB electrolytes, Si-graphene anode achieved more than 2000 $mAhg^{-1}$ at end of first discharge with a Coulombic efficiency of more than 80 %. Upon cycling, capacity drops rapidly and after 50 cycles it is around 67 % of initial capacity. Nevertheless, it should be noted that without the addition of IL, capacity drops down to 55 % after 50 cycles.

Based on the electrochemical characterization as well as the performance in lithium cell, the electrolyte based on $Pyr_{1,5}$TFSI resulted to be the most promising among the three ionic liquids analyzed. So, both PB and TB have been used to prove the feasibility to use of these kind of electrolytes in a complete Li-ion by facing to a commercial LFP cathode and a high-capacity anode such as Si-graphene composite (Figures 7 and S10). Overall satisfactory performance has been obtained thus confirming the applicability of the novel electrolyte blends here proposed. On passing we would like to stress that the benchmark LFP/Si-graphene cell assembled using a P electrolyte (IL-free) as expected failed in few cycles (data omitted) in line with the poor performances in both Si-graphene/Li and LFP/Li half cells (see above).

Optimization of electrode formulation and additives may further improve the final battery features: however this technological optimization is beyond the scope of this work.

3. Conclusions

Six different electrolytes have been prepared by adding the 50 wt.% of pyrrolidinium-based ionic liquids with 3 different alkyl chains, i.e. butyl- penthyl- and octyl- to 2 alkylcarbonate-based electrolytes, i.e. 1 M $LiPF_6$ in DMC:EC (P-series) and 1 M LiTFSI in DMC:EC (T-series). The influence of the length of the alkyl chain on the two series of electrolytes (i.e. P and T) have been studied.

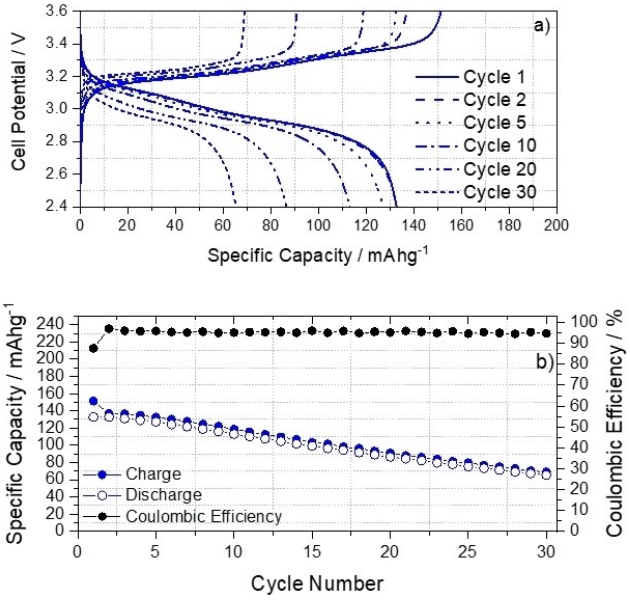

Figure 7. Room temperature galvanostatic charge-discharge measurements of LFP/Si-graphene cells at 100 mAg^{-1}: a) representative voltage profiles and b) cycling performance with PB electrolyte.

The IL-added solutions proved to have higher flash points than the pristine electrolytes, that increase with the length of alkyl chain. The latter is mostly evident in the P-series electrolytes, while in the T-series only moderate difference are noticeable. In the same way, viscosity increase with the cation size, due to the higher steric hindrance of octyl- group compared to butyl-. This is in line with the values observed for ionic conductivity, where the elongation of alkyl chain affects negatively the conductivity. Nevertheless, the value remains comparable to the pure carbonate-based electrolytes. The increase of the values of viscosity and ionic conductivity with the alkyl chain do not affect the ionicity, as showed in the Walden plot.

The physico-chemical properties of the six electrolytes have been related to microscopic changes in the local coordination in the liquid phase by Raman Spectroscopy. Differences in the vibrational modes, due to the pyrrolidinium cation can be detected only in the spectra of pure ionic liquids; while, in the electrolyte mixtures such vibrational modes are completely covered by the signals associated to organic solvents. By quantitative analysis, information about the average coordination number revealed that for all the electrolytes, Li^+ is coordinated mostly by EC and DMC anion; while only a small quantity, which is not influenced by the length of alkyl chain and remain constant, is coordinated by TFSI. As expected, Li^+ is coordinated preferentially by EC molecules, even though the P- and T-series electrolytes show some differences. In fact, it is evident that in the case of IL-added T-electrolytes we can observe that the Li–EC and Li–DMC coordination number decrease with the length of alkyl chain. This correlation is not obvious in the case of P-electrolytes. Probably, the presence of PF_6^- in addition to TFSI anion can influence the degree of coordination with Li-ions.

From the electrochemical point of view, all the electrolytes showed an electrochemical stability window above 5 V. For both the series a slight increase of electrochemical stability is visible passing from butyl to pentyl- while decrease with octyl-side chain. Also, IL added P electrolytes with shorter alkyl chain exhibited (PA and PB) enhanced properties compared to pure P as well as to T-series electrolytes. Once assembled in lithium half-cells vs. LFP, all electrolytes supplied reversible and stable cycling: PB and PT electrolytes outperform the other formulations and have been further investigated in lithium half cells vs. silicon-carbon composite (Si–C) electrodes. Furthermore, both electrolytes have been tested in full Li-ion configurations (LFP/Si–C) to demonstrate the applicability of these new electrolyte solutions at lab scale in complete devices.

Experimental Section

Sample preparation

1 M $LiPF_6$ in EC:DMC = 50:50 v/v (labeled as P), $Pyr_{1,4}TFSI$, $Pyr_{1,5}TFSI$ and $Pyr_{1,8}TFSI$ were purchased from solvionic and used as received. LiTFSI (Sigma Aldrich) was dried under vacuum for 3 days at 120 °C, while EC and DMC (Sigma Aldrich) were used as received. All the manipulations were carried out in an argon filled glove box having oxygen and humidity levels less than 0.1 ppm. For the preparation of T electrolytes (see following results and discussion and table 1 for the acronym definition), a 1:1 (v/v) mixture of EC and DMC was prepared and the mixture was left under molecular sieves for a week before the use. Then, LiTFSI was dissolved in EC:DMC solvent in order to have 1 M LiTFSI solution. Electrolyte solutions were prepared in a weight ratio between ionic liquid and electrolyte of 50:50, using $Pyr_{1,x}TFSI$ ionic liquid where $x = 3,5$ and 8. After the addition of ionic liquid to P or T electrolyte, the solution was mixed with a mechanical stirrer overnight.

Electrolytes characterization

The Flash points of the electrolytes solutions were determined by using a Grabner instrument and according to the measurement protocol D6450. 1 ml of sample heated in a closed cup from T (initial) to T(final). To follow the protocol exactly, T(initial) was equal to T(flash) minus 18 °C, while the T(final) was kept enough to detect the T(flash) of the solution. The heating rate was 5.5 °C min^{-1} and the ignition interval of 1 test per °C. The viscosity of the mixed electrolytes was determined by a Lovis 2000 M/ME (Anton Paar) viscosity meter in the temperature range 10 °C and 80 °C. The temperature was increased in steps of 10 °C. The ionic conductivity of the electrolytes solution was determined by dielectric measurements, performed with a Novocontrol GmBH broadband dielectric spectrometer equipped with a Quatro Cryosystem temperature control unit. The measurements were performed in the frequency range of 10^{-1}–10^7 Hz and temperature range between −10–60 °C, respectively. The temperature was increased in steps of 10 °C and at each temperature an equilibration time of 30 min was used. The fitting procedure of the temperature dependence of the ionic conductivity has been carried out by assuming either the VTF and the Arrhenius models. The fitting has been performed using a non-linear randomized fitting algorithm programmed on spreadsheet (e.g. Excel): the goal function was the minimum chi-square parameter calculated between experimental and fitted conductivity data.

Room temperature Raman scattering measurements were carried out using a Renishaw inVia micro-Raman spectrometer in back-scattering geometry equipped with 785 nm diode laser (power 82 mW) as the excitation light source. The electrolyte was inside a quartz Cuvette and the incident laser was focused by a 5X optical microscope objective with a numerical aperture of 0.14 and then the scattered light was detected in a back-scattering geometry dispersed by 1200 grooves mm^{-1} grating on CCD detector. Acquisition time for a single measurement was 5 sec.

The electrochemical stability window of all the electrolytes were evaluated by LSV for anodic scan and CV for cathodic scan, using SuperP carbon casted on aluminum (cathodic) or copper (anodic) foil as working electrode and a lithium foil as counter electrode. The voltage range used was 0–6 V for LSV and 0.005–2.5 V for CV, while the scan rate was 1 mV/s.

The lithium transference number was determined by potentiostatic-polarization measurements. Following the method proposed by Vincent, Bruce and Evans[61] a small potential of 50 mV has been applied between symmetric lithium/lithium cell for 1 hour or at least potential stabilization. Electrochemical impedance spectroscopy (EIS) has been used to monitored the resistance values before and after polarization. EIS measurements were performed applying a potential of 10 mV in the frequency range 100 kHz–100 mHz.

Galvanostatic deposition-stripping tests have been carried out in a symmetric Li/electrolyte/Li cell using a current density of 0.1 $mAcm^{-2}$ with a step duration of 30 minutes.

A Biologic VMP3 multichannel potentiostat has been used for all the measurements. All the tests have been carried out in Teflon coated Swagelok cells.

Electrochemical tests

A Biologic BCS-805 battery cycler has been used for galvanostatic cycling. Coin cells 2032 were assembled using $LiFePO_4$ (LFP) or Si/graphene as working and lithium foil as counter electrode. A Whatman glass fiber disk soaked with 100 µl of electrolyte was used as separator. For LFP, galvanostatic tests were carried out in a potential range of 2.5–3.8 V using a rate of C/10 (1 C = 170 mA g^{-1}); while for Si-graphene, galvanostic tests were performed between 0.01–2 V as formation cycle and between 0.1–1 V for the other cycles. $LiFePO_4$ electrode sheets with a nominal capacity of 2.3 mAh cm^{-2} were purchased from NEI Corporation. Si-graphene electrodes were prepared following the procedure described in Ref. [59], Ref. [60].

Finally, for Li-ion, tests were carried out between 2.4–3.6 V with a current density of 100 mA g^{-1}. The full cells were balanced considering the nominal capacity of the cathode and the reversible capacity of the anode, obtained from the galvanostatic tests in lithium cells.

Acknowledgements

A.C., S.P., J.K.P. and V.P. acknowledge the European Union's Horizon 2020 research and innovation program under grant agreement no. 785219, GrapheneCore2.

Conflict of Interest

The authors declare no conflict of interest.

Keywords: ionic liquids · mitigation of the irreversible capacity in Li-ion cells · non-aqueous electrolytes · Li-ion batteries

[1] P. G. Bruce, B. Scrosati, J. M. Tarascon, *Angew. Chem. Int. Ed.* **2008**, *47*, 2930–2946; *Angew. Chem.* **2008**, *120*, 2972–2989.
[2] M. Armand, J.-M. Tarascon, *Nature* **2008**, *451*, 652–657.
[3] J. Kalhoff, G. G. Eshetu, D. Bresser, S. Passerini, *ChemSusChem* **2015**, *8*, 2154–2175.
[4] M. Ue, S. Mori, *J. Electrochem. Soc.* **1995**, *142*, 2577.
[5] X. Zhang, B. Winget, M. Doeff, J. W. Evans, T. M. Devine, *J. Electrochem. Soc.* **2005**, *152*, B448.
[6] S. F. Lux, I. T. Lucas, E. Pollak, S. Passerini, M. Winter, R. Kostecki, *Electrochem. Commun.* **2012**, *14*, 47–50.
[7] T. Kawamura, S. Okada, J. ichi Yamaki, *J. Power Sources* **2006**, *156*, 547–554.
[8] A. Webber, *J. Electrochem. Soc.* **1991**, *138*, 2586.
[9] S. Sylla, J. Y. Sanchez, M. Armand, *Electrochim. Acta* **1992**, *37*, 1699–1701.
[10] V. Sharova, A. Moretti, T. Diemant, A. Varzi, R. J. Behm, S. Passerini, *J. Power Sources* **2018**, *375*, 43–52.
[11] M. Dahbi, F. Ghamouss, F. Tran-Van, D. Lemordant, M. Anouti, *J. Power Sources* **2011**, *196*, 9743–9750.
[12] L. J. Krause, W. Lamanna, J. Summerfield, M. Engle, G. Korba, R. Loch, R. Atanasoski, *J. Power Sources* **1997**, *68*, 320–325.
[13] K. Xu, *Chem. Rev.* **2004**, *104*, 4303–4417.
[14] D. Aurbach, Y. Talyosef, B. Markovsky, E. Markevich, E. Zinigrad, L. Asraf, J. S. Gnanaraj, H. J. Kim, *Electrochim. Acta*, Pergamon **2004**, pp. 247–254.
[15] M. Galiński, A. Lewandowski, I. Stepniak, *Electrochim. Acta* **2006**, *51*, 5567–5580.
[16] A. Lewandowski, A. Świderska-Mocek, *J. Power Sources* **2009**, *194*, 601–609.
[17] M. Agostini, A. Matic, S. Panero, F. Croce, R. Gunnella, P. Reale, S. Brutti, *Electrochim. Acta* **2017**, *235*, 262–269.
[18] M. Agostini, S. Brutti, M. A. Navarra, S. Panero, P. Reale, A. Matic, B. Scrosati, *Sci. Rep.* **2017**, *7*, 1104.
[19] S. Seki, Y. Kobayashi, H. Miyashiro, Y. Ohno, A. Usami, Y. Mita, N. Kihira, M. Watanabe, N. Terada, *J. Phys. Chem. B* **2006**, *110*, 10228–10230.
[20] G. B. Appetecchi, S. Scaccia, C. Tizzani, F. Alessandrini, S. Passerini, *J. Electrochem. Soc.* **2006**, *153*, A1685.
[21] M. Armand, F. Endres, D. R. MacFarlane, H. Ohno, B. Scrosati, *Nat. Mater.* **2009**, *8*, 621–629.
[22] H. Matsumoto, H. Sakaebe, K. Tatsumi, M. Kikuta, E. Ishiko, M. Kono, *J. Power Sources* **2006**, *160*, 1308–1313.
[23] H. Sakaebe, H. Matsumoto, K. Tatsumi, *J. Power Sources*, Elsevier **2005**, pp. 693–697.
[24] H. F. Xiang, B. Yin, H. Wang, H. W. Lin, X. W. Ge, S. Xie, C. H. Chen, *Electrochim. Acta* **2010**, *55*, 5204–5209.
[25] L. Larush, V. Borgel, E. Markevich, O. Haik, E. Zinigrad, D. Aurbach, G. Semrau, M. Schmidt, *J. Power Sources* **2009**, *189*, 217–223.
[26] B. Garcia, S. Lavallée, G. Perron, C. Michot, M. Armand, *Electrochim. Acta* **2004**, *49*, 4583–4588.
[27] M. Kunze, S. Jeong, G. B. Appetecchi, M. Schönhoff, M. Winter, S. Passerini, *Electrochim. Acta*, Pergamon **2012**, pp. 69–74.
[28] M. Montanino, M. Moreno, M. Carewska, G. Maresca, E. Simonetti, R. Lo Presti, F. Alessandrini, G. B. Appetecchi, *J. Power Sources* **2014**, *269*, 608–615.
[29] A. Guerfi, M. Dontigny, P. Charest, M. Petitclerc, M. Lagacé, A. Vijh, K. Zaghib, *J. Power Sources* **2010**, *195*, 845–852.
[30] I. Quinzeni, S. Ferrari, E. Quartarone, C. Tomasi, M. Fagnoni, P. Mustarelli, *J. Power Sources* **2013**, *237*, 204–209.
[31] B. S. Lalia, N. Yoshimoto, M. Egashira, M. Morita, *J. Power Sources* **2010**, *195*, 7426–7431.
[32] B. Yang, C. Li, J. Zhou, J. Liu, Q. Zhang, *Electrochim. Acta* **2014**, *148*, 39–45.
[33] A. Tsurumaki, M. A. Navarra, S. Panero, B. Scrosati, H. Ohno, *J. Power Sources* **2013**, *233*, 104–109.
[34] T. Sato, T. Maruo, S. Marukane, K. Takagi, *J. Power Sources* **2004**, *138*, 253–261.
[35] L. Lombardo, S. Brutti, M. A. Navarra, S. Panero, P. Reale, *J. Power Sources* **2013**, *227*, 8–14.
[36] L. T. M. Le, T. D. Vo, K. H. P. Ngo, S. Okada, F. Alloin, A. Garg, P. M. L. Le, *J. Mol. Liq.* **2018**, *271*, 769–777.
[37] G. H. Lane, A. S. Best, D. R. MacFarlane, M. Forsyth, P. M. Bayley, A. F. Hollenkamp, *Electrochim. Acta* **2010**, *55*, 8947–8952.
[38] K. Kim, Y. H. Cho, H. C. Shin, *J. Power Sources* **2013**, *225*, 113–118.
[39] The European Parliament and the Council of the European Union, REGULATION (EC) No 1272/2008 OF THE EUROPEAN PARLIAMENT and OF THE COUNCIL of 16 December 2008 on Classification, Labelling and Packaging of Substances and Mixtures, Amending and Repealing Directives 67/548/EEC and 1999/45/EC, and Amending Regulation (EC) **2008**.
[40] United Nations. Committee of Experts on the Transport of Dangerous Goods., United Nations. Economic Commission for Europe. Secretariat., United Nations **2010**, pp. 1–8.
[41] M. Taggougui, M. Diaw, B. Carré, P. Willmann, D. Lemordant, *Electrochim. Acta* **2008**, *53*, 5496–5502.
[42] K. Oldiges, D. Diddens, M. Ebrahiminia, J. B. Hooper, I. Cekic-Laskovic, A. Heuer, D. Bedrov, M. Winter, G. Brunklaus, *Phys. Chem. Chem. Phys.* **2018**, *20*, 16579–16591.
[43] L. Dagousset, G. T. M. Nguyen, F. Vidal, C. Galindo, P. H. Aubert, *RSC Adv.* **2015**, *5*, 13095–13101.
[44] A. Martinelli, A. Matic, P. Jacobsson, L. Börjesson, A. Fernicola, B. Scrosati, *J. Phys. Chem. B* **2009**, *113*, 11247–11251.
[45] K. M. Diederichsen, H. G. Buss, B. D. McCloskey, *Macromolecules* **2017**, *50*, 3831–3840.
[46] W. Xu, E. I. Cooper, C. A. Angell, *J. Phys. Chem. B* **2003**, *107*, 6170–6178.
[47] D. R. MacFarlane, M. Forsyth, E. I. Izgorodina, A. P. Abbott, G. Annat, K. Fraser, *Phys. Chem. Chem. Phys.* **2009**, *11*, 4962–4967.

[48] P. Walden, *Z. Phys. Chem. Suppl.* **1906**, *55 U*, DOI 10.1515/zpch-1906-5511.
[49] C. Schreiner, S. Zugmann, R. Hartl, H. J. Gores, *J. Chem. Eng. Data* **2010**, *55*, 1784–1788.
[50] R. Matsumoto, M. W. Thompson, P. T. Cummings, *J. Phys. Chem. B* **2019**, DOI 10.1021/acs.jpcb.9b08509.
[51] M. Kunze, S. Jeong, E. Paillard, M. Schönhoff, M. Winter, S. Passerini, *Adv. Energy Mater.* **2011**, *1*, 274–281.
[52] J. C. Lassègues, J. Grondin, R. Holomb, P. Johansson, *J. Raman Spectrosc.* **2007**, *38*, 551–558.
[53] M. Castriota, T. Caruso, R. G. Agostino, E. Cazzanelli, W. A. Henderson, S. Passerini, *J. Phys. Chem. A* **2005**, *109*, 92–96.
[54] J. Pitawala, A. Martinelli, P. Johansson, P. Jacobsson, A. Matic, *J. Non-Cryst. Solids* **2015**, *407*, 318–323.
[55] V. H. Paschoal, L. F. O. Faria, M. C. C. Ribeiro, *Chem. Rev.* **2017**, *117*, 7053–7112.
[56] A. Martinelli, A. Matic, P. Johansson, P. Jacobsson, L. Börjesson, A. Fernicola, S. Panero, B. Scrosati, H. Ohno, *J. Raman Spectrosc.* **2011**, *42*, 522–528.
[57] J. C. Lassègues, J. Grondin, D. Talaga, *Phys. Chem. Chem. Phys.* **2006**, *8*, 5629–5632.
[58] L. Aguilera, J. Scheers, A. Matic, *Phys. Chem. Chem. Phys.* **2016**, *18*, 25458–25464.
[59] E. Greco, G. Nava, R. Fathi, F. Fumagalli, A. E. Del Rio-Castillo, A. Ansaldo, S. Monaco, F. Bonaccorso, V. Pellegrini, F. Di Fonzo, *J. Mater. Chem. A* **2017**, *5*, 19306–19315.
[60] S. Palumbo, L. Silvestri, A. Ansaldo, R. Brescia, F. Bonaccorso, V. Pellegrini, *ACS Appl. Energy Mater.* **2019**, *2*, 1793–1802.
[61] J. Evans, C. A. Vincent, P. G. Bruce, *Polymer* **1987**, *28*, 2324–2328.

Manuscript received: April 2, 2020
Revised manuscript received: May 11, 2020
Accepted manuscript online: May 11, 2020
Version of record online: May 27, 2020